Journal of Theoretical Biology 487 (2020) 110123

Contents lists available at ScienceDirect

Journal of Theoretical Biology

journal homepage: www.elsevier.com/locate/jtb

Excitation states of metabolic networks predict dose-response fingerprinting and ligand pulse phase signalling

Jay S Coggan[a,*], Daniel Keller[a], Henry Markram[a], Felix Schürmann[a], Pierre J Magistretti[b]

[a] Blue Brain Project, École Polytechnique Fédérale de Lausanne (EPFL), Geneva CH-1202, Switzerland
[b] Biological and Environmental Sciences and Engineering Division, King Abdullah University of Science and Technology (KAUST), Thuwal 23955, Saudi Arabia

ARTICLE INFO

Article history:
Received 6 September 2019
Revised 8 November 2019
Accepted 16 December 2019
Available online 19 December 2019

Keywords:
Enzyme cascade
Phase signalling
Ligand pulse
Dose-response fingerprinting
Synthetic biology

ABSTRACT

With a computational model of energy metabolism in an astrocyte, we show how a system of enzymes in a cascade can act as a functional unit of interdependent reactions, rather than merely a series of independent reactions. These systems may exist in multiple states, depending on the level of stimulation, and the effects of substrates at any point will depend on those states. Response trajectories of metabolites downstream from cAMP-stimulated glycogenolysis exhibit a host of non-linear dynamical response characteristics including hysteresis and response envelopes. Dose-dependent phase transitions predict a novel intracellular signalling mechanism and suggest a theoretical framework that could be relevant to single cell information processing, drug discovery or synthetic biology. Ligands may produce unique dose-response fingerprints depending on the state of the system, allowing selective output tuning. We conclude with the observation that state- and dose-dependent phase transitions, what we dub "ligand pulses" (LPs), may carry information and resemble action potentials (APs) generated from excitatory postsynaptic potentials. In our model, the relevant information from a cAMP-dependent glycolytic cascade in astrocytes could reflect the level of neuromodulatory input that signals an energy demand threshold. We propose that both APs and LPs represent specialized cases of molecular phase signalling with a common evolutionary root.

1. Introduction

The long-standing inadequacy of our understanding of cells, from biochemistry to behaviour, from bacteria to neurons, has vexed the development of more effective treatments for many medical disorders, most notably those that lead to neurodegeneration. Various levels of biological complexity are usually fingered as the culprits, with expansive systems of interlocked biochemical cascades and cellular networks at the root of their nature. For example, ubiquitous intracellular signalling pathways in single cells work in parallel at multiple scales of space and time. The challenge of understanding phenomena such as aging in order to delay or circumvent senescence or any number of neuropathologies will likely require a leap forward in systems biology concepts (Kirkwood, 2011, Kowald and Kirkwood, 1996, Kriete et al., 2011, Mc Auley et al., 2017).

Second-messenger signalling can involve any number of cascading, enzyme-catalyzed steps whereby stimuli such as neuromodulators are transduced from one metabolite to another, each in turn capable of feeding another cascade. Elusive disease cures require an understanding that currently eludes traditional experimental designs and capabilities. Computational methods that complement laboratory techniques may provide this understanding.

Computational modelling of intracellular enzymatic cascades is a valuable tool for understanding single cell functions (Schoeberl et al., 2002). As a case in point, here we describe a novel analysis of a previously described model of energy metabolism and neuromodulation in glia (Coggan et al., 2018, Jolivet et al., 2015). We show how this approach can reveal insights not only about this particular pathway, but also make predictions about the behavior and previously unsuspected roles of second-messenger systems in general, since metabolic cascades are central to almost all cellular functions and dysfunctions (DeBerardinis and Thompson, 2012).

With the simple concept of excitability states of an enzymatic cascade stimulated, for example, by a neuromodulator such as norepinephrine, we are able to make predictions about their

* Corresponding author.
E-mail addresses: jay.coggan@epfl.ch (J.S. Coggan), daniel.keller@epfl.ch (D. Keller), henry.markram@epfl.ch (H. Markram), felix.schuermann@epfl.ch (F. Schürmann), pierre.magistetti@kaust.edu.sa (P.J. Magistretti).

https://doi.org/10.1016/j.jtbi.2019.110123

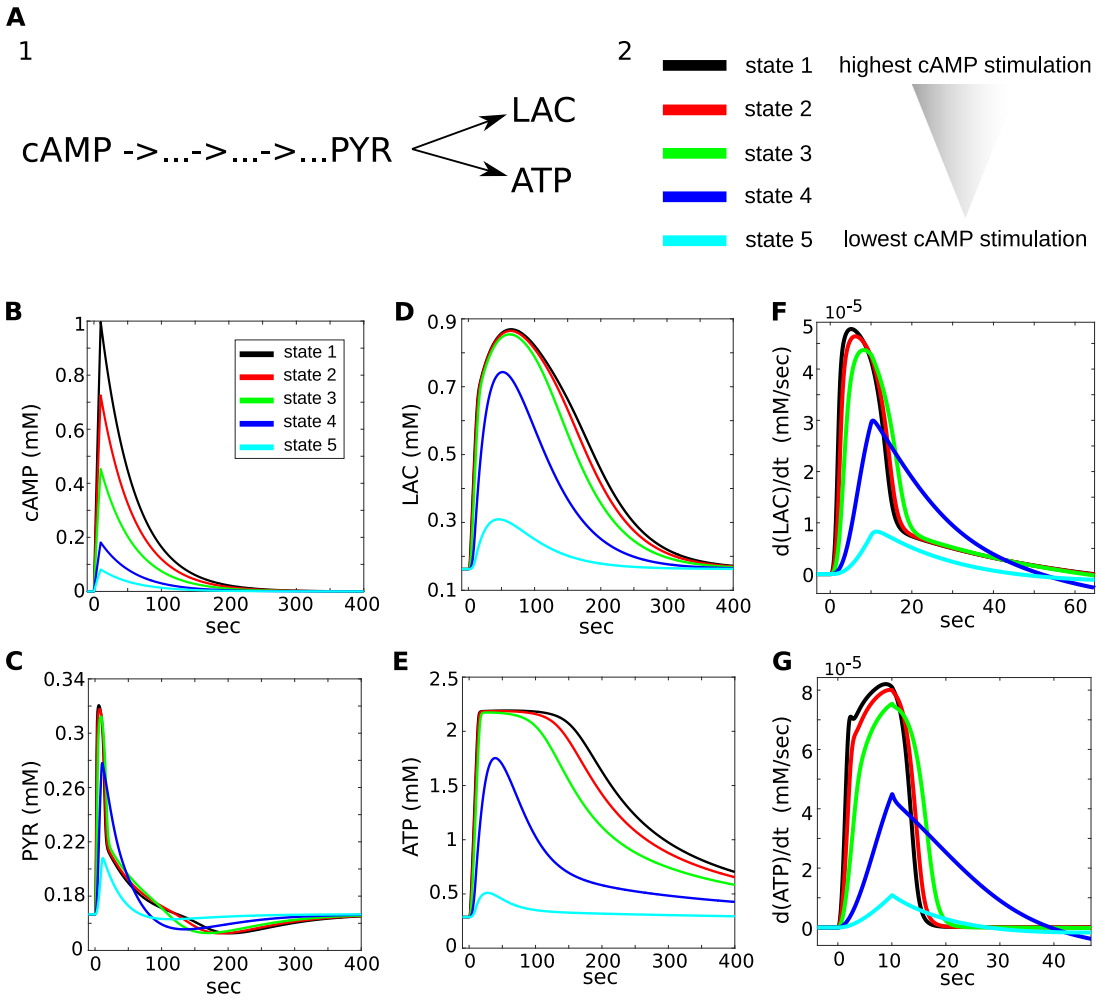

Fig. 1. Model summary and response trajectories of selected metabolites in 5 excitation levels of a metabolic enzyme cascade stimulated by 5 doses of cAMP. A) The metabolic cascade system, from cAMP to the pyruvate (PYR) bifurcation to lactate and ATP, is stimulated to 5 excitability states by 5 concentrations of cAMP. Trajectories of primary metabolites of interest B) cAMP, C) pyruvate (PYR), D) lactate (LAC), E) ATP. The phase transitions occur in the concentration step between states 3 and 4. F, G) Derivative phase plots show phase transition between lower (cyan, blue) and higher (green, red, black) excitability states, corresponding to concentrations of cAMP. Examples made of LAC and ATP.

properties and behavior. We observed that, depending on the state of metabolic excitation, each metabolite concentration may cycle through a set of stereotyped responses to the rise and fall of cAMP concentrations. These responses may include patterns of hysteresis, response envelopes and phase transitions.

Phase transitions (defined here as a thermodynamic shift in the state or properties of a system of reactions) among intracellular reactions play a role in normal and pathological cell physiology (Nedelsky and Taylor, 2019, Tsuruyama, 2014), including energy production pathways such as glycolysis (Mulukutla et al., 2015). We find that excitation state-dependent, hysteretic, phase plots yield rich information about the behavior of an enzymatic cascade. Furthermore, we make the theoretical proposition that understanding the effect of a drug on a biological system requires knowledge of the state of the entire system.

We further hypothesize that both ligand pulses (LPs) and action potentials (APs) represent specialized cases of molecular phase signalling (MPS), and suggest that APs might be late evolutionary adaptations of more ancient and established intracellular MPS mechanisms for the purpose of long-range communication and information processing in nervous systems (Boyer and Wisniewski-Dyé, 2009).

Our results exemplify how a large-scale biomolecular simulation such as the one being built at the Blue Brain Project can be employed as a platform for theoretical advancements in understanding complex molecular systems. Beyond understanding normal physiology, simulation science will also play an increasingly fundamental role in the burgeoning discipline of synthetic biology, a field that seeks to understand and manipulate catabolic and anabolic pathways that might improve the yield of useful metabolites (Mulukutla et al., 2016, Erb et al., 2017), or engineer *de novo* pathways for the production of high-value compounds (Martin et al., 2009).

2. Methods

The model used in this paper is based on that previously published (Coggan et al., 2018, Jolivet et al., 2015). Here, we focus on a segment of the deterministic cascade between cAMP production (as stimulated by 5 levels of noradrenergic activation of the β2-adrenergic receptor as in (Coggan et al., 2018)) with each colored plot coming from an independent simulation with a different concentration of cAMP and outputs of the pyruvate (PYR) bifurcation, lactate (LAC) and ATP (cAMP → ... PYR→ LAC, ATP). The five relatively equally spaced stimulation levels of cAMP were chosen as a dose-response regimen with which to stimulate the enzyme system to a range of levels of excitation roughly corresponding to the dose-response range for cAMP in this system. These levels are

Table 1
Governing equations

Variable	Value at rest	Equation	
Intracellular sodium	8/15 mM	$\frac{d}{dt}\,Na_x^+ = J^x_{leak,Na} - 3\,J^x_{pump} + J^x_{stim}(t)$	*(1)
Neuronal glucose	1.2 mM	$\frac{d}{dt}\,GLC_n = J^{en}_{GLC} - J^n_{HKPFK}$	(2)
Astrocytic glucose	1.19 mM	$\frac{d}{dt}\,GLC_g = J^{cg}_{GLC} + J^{eg}_{GLC} - J^g_{HKPFK}$	(3)
Glyceraldehyde-3-phosphate	0.0046 mM	$\frac{d}{dt}\,GAP_x = 2\,J^x_{HKPFK} - J^x_{PGK} + vL3 - v\_3$	(4)
Phosphoenolpyruvate	0.015 mM	$\frac{d}{dt}\,PEP_x = J^x_{PGK} - J^x_{PK}$	(5)
Pyruvate	0.17 mM	$\frac{d}{dt}\,PYR_x = J^x_{PK} - J^x_{LDH} - J^x_{mito,\ in}$	(6)
Neuronal lactate	0.6 mM	$\frac{d}{dt}\,LAC_n = J^n_{LDH} - J^{ne}_{LAC}$	(7)
Astrocytic lactate	0.6 mM	$\frac{d}{dt}\,LAC_g = J^g_{LDH} - J^{ge}_{LAC} - J^{gc}_{LAC}$	(8)
Cytosolic NADH †	0.006/0.1 mM	$\frac{d}{dt}\,NADH^{cyto}_x = (1-\xi)^{-1}(J^x_{PGK} - J^x_{LDH} - J^x_{shuttle})$	(9)
Mitochondrial NADH †	0.12 mM	$\frac{d}{dt}\,NADH^{mito}_x = \xi^{-1}(4\,J^x_{mito,in} - J^x_{mito,out} + J^x_{shuttle})$	(10)
Neuronal ATP ‡	2.2 mM	$\frac{d}{dt}\,ATP_n = (-2\,J^n_{HKPFK} + J^n_{PGK} + J^n_{PK} - J^n_{ATPases} - J^n_{pump} + 3.6\,J^n_{mito,out} + J^n_{CK})(1 - \frac{dAMP_n}{dATP_n})^{-1}$	(11)
Astrocytic ATP ‡	2.2 mM	$\frac{d}{dt}\,ATP_g =$ $(-2\,J^g_{HKPFK} + J^g_{PGK} + J^g_{PK} - J^g_{ATPases} - \frac{7}{4}\,J^g_{pump} + \frac{3}{4}\,J^g_{pump,0} + 3.6\,J^g_{mito,out} + J^g_{CK})(1 - \frac{dAMP_g}{dATP_g})^{-1}$	(12)
Phosphocreatine	4.9 mM	$\frac{d}{dt}\,PCr_x = -J^x_{CK}$	(13)
Neuronal oxygen	0.028 mM	$\frac{d}{dt}\,O_{2n} = J^{cn}_{O_2m} - 0.6\,J^n_{mito,out}$	(14)
Astrocytic oxygen	0.028 mM	$\frac{d}{dt}\,O_{2g} = J^{cg}_{O_2m} - 0.6\,J^g_{mito,out}$	(15)
Capillary oxygen	7 mM	$\frac{d}{dt}\,O_{2c} = J^c_{O_2} - 1/r_{cn}\,J^{cn}_{O_2m} - 1/r_{cg}\,J^{cg}_{O_2m}$	(16)
Capillary glucose	4.5 mM	$\frac{d}{dt}\,GLC_c = J^c_{GLC} - 1/r_{ce}\,J^{ce}_{GLC} - 1/r_{cg}\,J^{cg}_{GLC}$	(17)
Capillary lactate	0.55 mM	$\frac{d}{dt}\,LAC_c = J^c_{LAC} + 1/r_{ce}\,J^{ec}_{LAC} + 1/r_{cg}\,J^{gc}_{LAC}$	(18)
Venous volume	0.02	$\frac{d}{dt}\,V_v = F_{in}(t) - F_{out}$	*(19)
Deoxyhemoglobin	0.058 mM	$\frac{d}{dt}\,dHb = F_{in}(t)\ (O_{2a} - O_{2\bar{c}}) - F_{out}\ \frac{dHb}{V_v}$	*(20)
Extracellular glucose	2.48 mM	$\frac{d}{dt}\,GLC_e = J^{ce}_{GLC} - 1/r_{eg}\,J^{eg}_{GLC} - 1/r_{en}\,J^{en}_{GLC}$	(21)
Extracellular lactate	0.6 mM	$\frac{d}{dt}\,LAC_e = 1/r_{en}\,J^{ne}_{LAC} + 1/r_{eg}\,J^{ge}_{LAC} - J^{ec}_{LAC}$	(22)
Neuronal membrane voltage	−73 mV	$\frac{d}{dt}\,\psi_n = C_m^{-1}(-I_L - I_{Na} - I_K - I_{Ca} - I_{mAHP} - I_{pump} + I_{syn}(t))$	*(23)
h gating variable	0.99	$\frac{d}{dt}\,h = \frac{\phi_h}{\tau_h}(h_\infty - h)$	(24)
n gating variable	0.02	$\frac{d}{dt}\,n = \frac{\phi_n}{\tau_n}(n_\infty - n)$	(25)
Neuronal calcium	5 10^{-5} mM	$\frac{d}{dt}\,Ca^{2+} = -\frac{S_m V_n}{F} I_{Ca} - 1/\tau_{Ca}(Ca^{2+} - Ca_0^{2+})$	(26)
Glycogen Module			
Glycogen-G6P equilibria		$vL1 = \frac{(k\_L1)(gluc)}{km\_L1+gluc}$	(27)
		$v\_L1 = \frac{(k\_L1)(G6P)}{km\_L1+G6P}$	(28)
		$vL2 = \frac{(kl2)(GSa)(G6P)}{kmL2+G6P}$	(29)
		$v\_L2 = \frac{(k\_L2)(glyc)}{km\_L2+glyc}$	(30)
Glycogenolytic glucose		$\frac{d}{dt}\,gluc = vtL1 - vL1 + v\_L1$	(31)
Glycogen		$\frac{d}{dt}\,glyc = vL2 - v\_L2$	(32)
Glucose 6-phosphate		$\frac{d}{dt}\,G6P = vL1 - v\_L1 - vL2 + v\_L2$	(33)
Blood glucose influx rate		$vtL1 = ktL1(B_{gluc} - gluc) = 0$	(34)
Blood glucose derivative		$\frac{d}{dt}\,B_{gluc} = 0$	(35)
cAMP	−−	$\frac{d}{dt}\,cAMP = (x(\frac{ne}{kDne+ne}) + y((\frac{1}{\tau_{cAMP}})(\frac{hb-ha}{1+(\frac{hc}{hk})^{hd}}) + (\frac{ha}{\tau_{cAMP}})) - 2\times kcg1\times R2C2\times(cAMP)^2 + 2\times k\_cg1\times R2CcAMP\times C - 2\times kgc2\times R2CcAMP2\times(cAMP)^2 + 2\times k\_cg2\times R2cAMP4\times C) - cAMP/\tau_{cAMP}\{x=\geq 0; y=\geq 0\}$	(36)
Glycogen Phosphorylase		$\frac{d}{dt}\,GPa = (\frac{((kg5)(PKa)(pt-GPa))}{kmg5(1+\frac{(s1)(G6P)}{kg2})+(pt-GPa)}) - (\frac{((kg6)(PP1+PP1_{GPa})(GPa))}{\frac{kmg6}{(1+\frac{(s2)(gluc)}{kg}}+(GPa)}) - (k_a)(PP1)(GPa) + (k\_a)(PP1_{GPa})$	(37)
Glycogen Synthase		$\frac{d}{dt}\,GSa = (\frac{((kg8)(PP1)(st-GPa))}{\frac{kmg8}{(1+\frac{(s1)(G6P)}{kg2})}+st-(GSa)}) - (\frac{((kg7)(PKa+C)(GSa))}{kmg7(1+\frac{(s1)(G6P)}{kg2})+(GSa)})$	(38)
Protein Phosphatase 1		$\frac{d}{dt}\,PP1 = (-k_a)(PP1)(GPa) + (k\_a)(PP1_{GPa})$	(39)
PP1-GPa		$\frac{d}{dt}\,PP1_{GPa} = (k_a)(PP1)(GPa) + (k\_a)(PP1_{GPa})$	(40)
Protein Kinase A		$\frac{d}{dt}\,PKa = (\frac{(kg3)(C)(kt-PKa)}{kmg3+kt-PKa}) - (\frac{((kg4)(PP1+PP1_{GPa})(PKa))}{kmg4+PKa})$	(41)
cAMP-dependent kinase cassette		$\frac{d}{dt}\,R2C2 = (-k_{gc1})(R2C2)(cAMP^2) + (k_{\_gc1})(R2CcAMP2)(C)$	(42)
""		$\frac{d}{dt}\,C = (k_{gc1})(R2C2)(cAMP^2) - (k_{\_gc1})(R2CcAMP2)(C) + (k_{gc2})(R2CcAMP2)(cAMP^2) - (k_{\_gc2})(R2CcAMP4)(C)$	(43)
""		$\frac{d}{dt}\,R2CcAMP2 = (k_{gc1})(R2C2)(cAMP^2) - (k_{\_gc1})(R2CcAMP2)(C) - (k_{gc2})(R2CcAMP2)(cAMP^2) + (k_{\_gc2})(R2CcAMP4)(C)$	(44)
""		$\frac{d}{dt}\,R2CcAMP4 = (k_{gc2})(R2CcAMP2)(cAMP^2) - (k_{\_gc2})(R2CcAMP4)(C)$	(45)
Dynamic equilibrium constant for glycogen degradation		$kd = (kmaxd - kmind)(\frac{1}{1+\frac{glyc}{kd_{mg}}^{\pi}}) + kmind$	(46)
Forward reaction rate for glycogen degradation		$k_a = \frac{k_{-a}}{kd}$	(47)
Cell energy charge		$CE = \frac{(ATP+\frac{ADP}{2})}{(ATP+ADP+AMP)}$	(48)
Cell oxidative status		$CO = \frac{[NAD^+]}{[NADH]}$	(49)
Neuromodulation Module			
Rise time constants for NE		$\tau_{ne1} = 10$ ms	(50)
Decay time constant for NE		$\tau_{ne2} = 500000$	(51)
Norepinephrine waveform		$NE = e^{-(t-tstim)/\tau ne2} - e^{-(t-tstim)/\tau ne1}$	(52)

* When two values are indicated, the first one corresponds to the neuronal compartment and the second one to the astrocytic compartment.

Table 2
Rates, transports and currents

Reaction, transport or current	Equation	
Sodium leak	$J^x_{leak,Na} = \frac{S_m V_x}{F}\ g^x_{Na}[\frac{RT}{F}\log(Na^+_e/Na^+_x) - \psi_x]$	(53)
Na,K-ATPase	$J^x_{pump} = S_m V_x\ k^x_{pump}\ ATP_x Na^+_x (1 + \frac{ATP_x}{K_{m,pump}})^{-1}$	(54)
Glucose transport	$J^{xy}_{GLC} = T^{xy}_{max,\ GLC}(\frac{GLC_x}{GLC_x + K^{xy}_{t,\ GLC}} - \frac{GLC_y}{GLC_y + K^{xy}_{t,\ GLC}})$	(55)
Hexokinase-phosphofructokinase	$J^x_{HKPFK} = k^x_{HKPFK}\ ATP_x \frac{GLC_x}{GLC_x + K_g}[1 + (\frac{ATP_x}{K_{i,ATP}})^{nH}]^{-1}$, GLCx = GLCg+g6p (astrocyte)	(56)
Phosphoglycerate kinase	$J^x_{PGK} = k^x_{PGK}\ \ GAP_x\ \ ADP_x(N - NADH^{cyto}_x)/NADH^{cyto}_x$	(57)
Pyruvate kinase	$J^x_{PK} = k^x_{PK}\ PEP_x\ ADP_x$	(58)
Lactate dehydrogenase	$J^x_{LDH} = k^{x+}_{LDH}\ PYR_x\ NADH^{cyto}_x - k^{x-}_{LDH}\ PYR_x\ (N - NADH^{cyto}_x)$	(59)
Lactate transport	$J^{xy}_{LAC} = T^{xy}_{max,\ LAC}(\frac{LAC_x}{LAC_x + K^{xy}_{t,\ LAC}} - \frac{LAC_y}{LAC_y + K^{xy}_{t,\ LAC}})$	(60)
TCA cycle	$J^x_{mito,in} = V^x_{max,\ in}\ \frac{PYR_x}{PYR_x + K^{mito}_m}\ \frac{N - NADH^{mito}_x}{N - NADH^{mito}_x + K^x_{m,NAD}}$	(61)
Electron transport chain	$J^x_{mito,out} = V^x_{max,\ out}\ \frac{O_{2x}}{O_{2x} + K^{mito}_{O_2}}\ \frac{ADP_x}{ADP_x + K^x_{m,ADP}}\ \frac{NADH^{mito}_x}{NADH^{mito}_x + K^x_{m,NADH}}$	(62)
NADH shuttles	$J^x_{shuttle} = T^x_{NADH}\ \frac{R^-_x}{R^-_x + M^{cyto}_x}\ \frac{R^+_x}{R^+_x + M^{mito}_x}$	(63)†
Creatine kinase	$J^x_{CK} = k^{x+}_{CK}\ ADP_x PCr_x - k^{x-}_{CK}\ ATP_x\ (C - PCr_x)$	(64)
Oxygen exchange	$J^{cx}_{O_2 m} = \frac{PS_{cap}}{V_x}(K_{O_2}(\frac{Hb.OP}{O_{2c}} - 1)^{-1/nh} - O_{2n})$	(65)
Capillary oxygen flow	$J^c_{O_2} = \frac{2F_{in}(t)}{V_{cap}}(O_{2a} - O_{2c})$	(66)
Capillary glucose flow	$J^c_{GLC} = \frac{2F_{in}(t)}{V_{cap}}(GLC_a - GLC_c)$	(67)
Capillary lactate flow	$J^c_{LAC} = \frac{2F_{in}(t)}{V_{cap}}(LAC_a - LAC_c)$	(68)
Oxygen concentration at the end of the capillary	$O_{2\bar{c}} = 2\ O_{2c} - O_{2a}$	(69)
Leak current	$I_L = g_L\ (\psi_n - E_L)$	(70)
Sodium current	$I_{Na} = g_{Na}\ m^3_\infty\ h(\psi_n - \frac{RT}{F}\log(Na^+_e/Na^+_n))$	(71)‡
Potassium current	$I_K = g_K n^4(\psi_n - E_K)$	(72)‡
Calcium current	$I_{Ca} = g_{Ca} m^2_{Ca}(\psi_n - E_{Ca})$	(73)‡
Calcium-dependent potassium current	$I_{mAHP} = g_{mAHP}\frac{Ca^{2+}}{Ca^{2+} + K_D}(\psi_n - E_K)$	(74)
Na,K-ATPase current	$I_{pump} = F k^n_{pump} ATP_n (Na^+_n - Na^+_0)\ (1 + \frac{ATP_x}{K_{m,pump}})^{-1}$	(75)
Flow out of the venous balloon	$F_{out} = F_0[(\frac{V_v}{V_{v0}})^{1/\alpha_v} + \frac{\tau_v}{V_{v0}}(\frac{V_v}{V_{v0}})^{-1/2}\frac{dV_v}{dt}]$, $F_0 = 0$	(76)

† With $R^-_x = NADH^{cyto}_x/(N - NADH^{cyto}_x)$ and $R^+_x = (N - NADH^{mito}_x)/NADH^{mito}_x$.
‡ Further equations in the Hodgkin-Huxley model are: $\alpha_m = -0.1\ \ (\psi_n + 33)/(\exp[-0.1\ \{\psi_n + 33\}] - 1)$, $\beta_m = 4\exp[-\{\psi_n + 58\}/12]$, $\alpha_h = 0.07\exp[-\{\psi_n + 50\}/10]$, $\beta_h = 1/(\exp[-0.1\{\psi_n + 20\}] + 1)$, $\alpha_n = -0.01\ \ (\psi_n + 34)/(\exp[-0.1\ \{\psi_n + 34\}] - 1)$, $\beta_n = 0.125\exp[-\{\psi_n + 44\}/25]$, $m_\infty = \alpha_m(\alpha_m + \beta_m)^{-1}$, $n_\infty = \alpha_n(\alpha_n + \beta_n)^{-1}$, $h_\infty = \alpha_h(\alpha_h + \beta_h)^{-1}$, $\tau_n = 10^{-3}(\alpha_n + \beta_n)^{-1}$, $\tau_h = 10^{-3}(\alpha_h + \beta_h)^{-1}$, $m_{Ca} = 1/(1 + \exp[-\{\psi_n + 20\}/9])$ and $E_L = (g^{pas}_K + g^n_{Na})^{-1}[g^{pas}_K E_K + g^n_{Na}\frac{RT}{F}\log(Na^+_e/Na^+_n)]$.

termed "states" and range from 1-5 in descending amplitude (with 1 being the highest and 5 the lowest, Fig 1A).

All enzyme cascade simulations were carried-out in NEURON, using a fixed time step of 3 μs with Euler integration, and was run either on an Ubuntu 14.04 LTS workstation with a 3.6 GHz Intel Core i7-4790 CPU and 15.6 GB RAM, or on the Blue Gene/Q in Lugano, Switzerland. Matlab was used for data analysis. AP and EPSP simulations were performed on the EPFL Blue Brain IV BlueGene/Q hosted at the Swiss National Supercomputing Center (CSCS) in Lugano. Parameters and equations for the NEURON simulation environment model are listed in Tables 1 (Governing equations), 2 (Rates, transports and currents), and 3 (parameters). The 5 concentrations of cAMP corresponding to cascade stimulation states 1–5 were obtained by setting x = 0.000009, 0.00002, 0.00005, 0.00008, or 0.00011 in Eq. (36) in Table 1.

3. Results

In this study, we made use of glycogenolysis and the subsequent glycolytic cascade from a previously published model of energy metabolism in glia (Coggan et al., 2018) to demonstrate the usefulness of a novel theoretical analysis of the characteristics and behavioral properties of a set of enzymatic reactions.

This segment of the metabolic energy cascade in our astrocyte model was stimulated into five excitability states by simulating the production of 5 concentrations of the second messenger cAMP (representing 5 levels of noradrenergic activation of the β2-adrenergic receptor as in (Coggan et al., 2018)). Diagramatically (Fig. 1A1), the arrows between cAMP and PYR represent the enzyme sequence protein kinase A (PKa), protein phosphatase 1 (PP1), glycogen phosphorylase (GPa), glycogen synthase (GSa), phosphoglucokinase (PGK), pyruvate kinase (PK), and lactate dehydrogenase (LDH); as well as the intermediate metabolites glucose-6-phosphate (G6P), glyceraldehyde phosphate (GAP), and phosphoenolpyruvate (PEP). The trajectories of selected metabolites cAMP, PYR, LAC and ATP are shown in Fig. 1, B–E, respectively. Derivative phase plots are another way to demonstrate the phase transition between lower (cyan, blue) and higher (green, red, black) excitability states, corresponding to concentrations of cAMP and examples made of LAC (Fig. 1F) and ATP (Fig. 1G).

3.1. Excitation-state phase plots

We examined the relationship between cAMP (the upstream trigger for the enzyme cascade we are analyzing) and a sample of several downstream intermediate metabolites (the "X" in the panel title). Plotting the relationship between cAMP and selected downstream metabolites (cAMP → X) yields a type of phase plot (Fig. 2A). Each colored plot is generated from an independent simulation with a different concentration of cAMP. These plots show different kinds of relationships varying from essentially no hysteresis (for cAMP vs. G6P, meaning [G6P] closely follows [cAMP]) and a variety of different hysteresis shapes for other metabolites. Characteristics of these plots include the close following by the concentration of a downstream metabolite to the concentration excursion of cAMP, as in the case of [cAMP] vs. [G6P] (the G6P concentration mirrors the cAMP concentration without significant deviation), or a variety of hysteresis types (all other responses in Fig. 2A) with apparent response envelopes of various shapes into which the responses "grow" and are contained with higher excitation states. These response envelopes thereby allow prediction of future states.

It is observed that the shapes of the curves qualitatively change between the two lowest states (cyan and blue) and the higher states (green, red and black), just as the transition between states

Table 3
Parameters.

Fixed parameters	
Volume fractions	$V_e = 0.2$, $V_{cap} = 0.0055$, $V_g = 0.25$, $V_n = 0.45$, $\xi = 0.07$, $r_{en} = V_e/V_n$, $r_{eg} = V_e/V_g$, $r_{ce} = V_{cap}/V_e$, $r_{cg} = V_{cap}/V_g$, $r_{cn} = V_{cap}/V_n$
Surface-to-volume ratios	$S_m V_n = 2.5\ 10^4$, $S_m V_g = 2.5\ 10^4$ cm^{-1}
Physical constants	$R = 8.31451$ J mol^{-1} K^{-1}, $F = 9.64853\ 10^4$ C mol^{-1}, $RT/F = 26.73$ mV, $\psi_g = -70$ mV, $Na_e^+ = 150$ mM
Glucose exchange affinities	$K_{t,GLC}^{en} = 8$, $K_{t,GLC}^{eg} = 8$, $K_{t,GLC}^{cg} = 8$, $K_{t,GLC}^{ce} = 8$ mM
Lactate exchange affinities	$K_{t,LAC}^{en} = 0.74$, $K_{t,LAC}^{ge} = 3.5$, $K_{t,LAC}^{gc} = 1$, $K_{t,LAC}^{ec} = 1$ mM
Hexokinase-phosphofructokinase system	$K_{I,ATP} = 1$ mM, $nH = 4$, $K_g = 0.05$ mM
Oxygen exchange constants	$K_{O_2} = 0.0361$ mM, $Hb.OP = 8.6$ mM, $nh = 2.73$
Electron transport chain	$K_{O_2}^{mito} = 0.001$ mM
Hodgkin-Huxley parameters	$C_m = 10^{-3}$ mF cm^{-2}, $g_L = 0.02$, $g_{Na} = 40$, $g_K = 18$, $g_{Ca} = 0.02$, $g_{mAHP} = 6.5$ mS cm^{-2}, $K_D = 30\ 10^{-3}$ mM, $\tau_{Ca} = 150\ 10^{-3}$ s, $Ca_0^{2+} = 0.5\ 10^{-4}$ mM, $E_K =$ -80, $E_{Ca} = 120$ mV, $\phi_n = \phi_h = 4$
Venous balloon	$\tau_v = 35$ s, $\alpha_v = 0.5$
Blood flow contribution to capillary glucose and oxygen	$O_{2a} = 8.35$, $GLC_a = 4.75$ mM
Na,K-ATPase and sodium leak	$g_{Na}^n = 0.0136$, $g_{Na}^g = 0.0061$, $g_K^{pas} = 0.2035$ mS cm^{-2}, $k_{pump}^n = 2.2\ 10^{-6}$, $k_{pump}^g = 4.5\ 10^{-7}$ cm mM^{-1} s^{-1}, $J_{pump,0}^g = 0.0687$ mM s^{-1}, $K_{m,pump} = 0.5$ mM
Total creatine plus phosphocreatine concentration	$C = 10$ mM
Total nicotinamide adenine dinucleotide concentration	$N = 0.212$ mM
TCA cycle	$K_m^{mito} = 0.04$ mM
Optimized parameters	
Lactate dehydrogenase	$k_{LDH}^{n+} = 72.3$, $k_{LDH}^{g+} = 1.59$ mM^{-1} s^{-1}
NADH shuttles	$M_n^{cyto} = 4.9\ 10^{-8}$, $M_g^{cyto} = 2.5\ 10^{-4}$, $M_n^{mito} = 3.93\ 10^5$, $M_g^{mito} = 1.06\ 10^4$
Electron transport chain	$K_{m,ADP}^n = 3.41\ 10^{-3}$, $K_{m,ADP}^g = 0.483\ 10^{-3}$, $K_{m,NADH}^n = 4.44\ 10^{-2}$, $K_{m,NADH}^g = 2.69\ 10^{-2}$ mM
Creatine kinase	$k_{CK}^{n+} = 0.0433$, $k_{CK}^{g+} = 0.00135$ mM^{-1} s^{-1}
TCA cycle	$K_{m,NAD}^n = 0.409$, $K_{m,NAD}^g = 40.3$ mM
Constrained parameters	
Glucose exchange constants	$T_{max,GLC}^{en} = 0.041$, $T_{max,GLC}^{ce} = 0.239$, $T_{max,GLC}^{eg} = 0.147$, $T_{max,GLC}^{cg} = 0.0016$ mM s^{-1}
Lactate exchange constants	$T_{max,LAC}^{gc} = 0.00243$, $T_{max,LAC}^{ne} = 24.3$, $T_{max,LAC}^{ge} = 106.1$, $T_{max,LAC}^{ec} = 0.25$ mM s^{-1}
Hexokinase-phosphofructokinase system	$k_{HKPFK}^n = 0.0504$, $k_{HKPFK}^g = 0.185$ s^{-1}
Lactate dehydrogenase	$k_{LDH}^{n-} = 0.72$, $k_{LDH}^{g-} = 0.071$ mM^{-1} s^{-1}
Oxygen exchange constants	$\frac{PS_{cap}}{V_n} = 1.66$, $\frac{PS_{cap}}{V_g} = 0.87$ s^{-1}
Electron transport chain	$V_{max,out}^n = 0.164$, $V_{max,out}^g = 0.064$ mM s^{-1}
TCA cycle	$V_{max,in}^n = 0.1303$, $V_{max,in}^g = 5.7$ mM s^{-1}
Phosphoglycerate kinase	$k_{PGK}^n = 3.97$, $k_{PGK}^g = 135.2$ mM^{-1} s^{-1}
Pyruvate kinase	$k_{PK}^n = 36.7$, $k_{PK}^g = 401.7$ mM^{-1} s^{-1}
ATPases	$J_{ATPases}^n = 0.1695$, $J_{ATPases}^g = 0.1404$ mM s^{-1}
Creatine kinase	$k_{CK}^{n-} = 0.00028$, $k_{CK}^{g-} = 10^{-5}$ mM^{-1} s^{-1}
NADH shuttles	$T_{NADH}^n = 10330$, $T_{NADH}^g = 150$ mM s^{-1}
Blood flow contribution to capillary lactate	$LAC_a = 0.506$ mM
Glycogen and NE related parameters	
kL1	0.05 mM/s
kL2	0.1 s^{-1}
kL3	0.002 mM/s
k_L1	0.07 mM/s
k_L2	0.1 s^{-1}
k_L3	0.002 mM/s
kmL1	7.7 mM
kmL2	0.57 mM
kmL3	0.01 mM
km_L1	1.3 mM
km_L2	1.4 mM
km_L3	0.0034 mM
ktL1	0.16 s^{-1}
kDne	3.0×10^{-4} mM
kgc1	1×10^{-6} s^{-1}
kgc2	1×10^{-6} s^{-1}
K_gc1	1×10^{-2} s^{-1}
K_gc2	1×10^{-2} s^{-1}
τ_{cAMP}	2.5 s
kg5	20 s^{-1}
kg6	5 s^{-1}
pt	0.07 mM
s1	100
s2	0.001
K_a	1 s^{-1} mM^{-1}
kgi	10 mM
kg7	20 mM

(*continued on next page*)

Table 3 (*continued*)

kg8	5 mM
kmg7	0.015
kmg8	0.00012
kg2	0.5 mM
kt	0.0025 mM
kg3	20 s^{-1}
kg4	5 s^{-1}
kmg3	0.004 mM
kmg4	0.0011 mM
kmaxd	3.2×10^{-3} mM
kmind	2.0×10^{-6} mM
Kd_mg	1 mM
τ_{ne1}	0.1, 1, 10 s
τ_{ne2}	500 s
cyclase coefficient 1	50×10^{-4}
cyclase coefficient 2	40×10^{-4}
cyclase coefficient 3	25×10^{-4}
cyclase coefficient 4	17×10^{-4}
Diffusion coefficient, NE	0.077×10^{-5} cm^2/s
Release site density	$2.1 \times 10^6/mm^3$
Gap, extracellular	30 nm

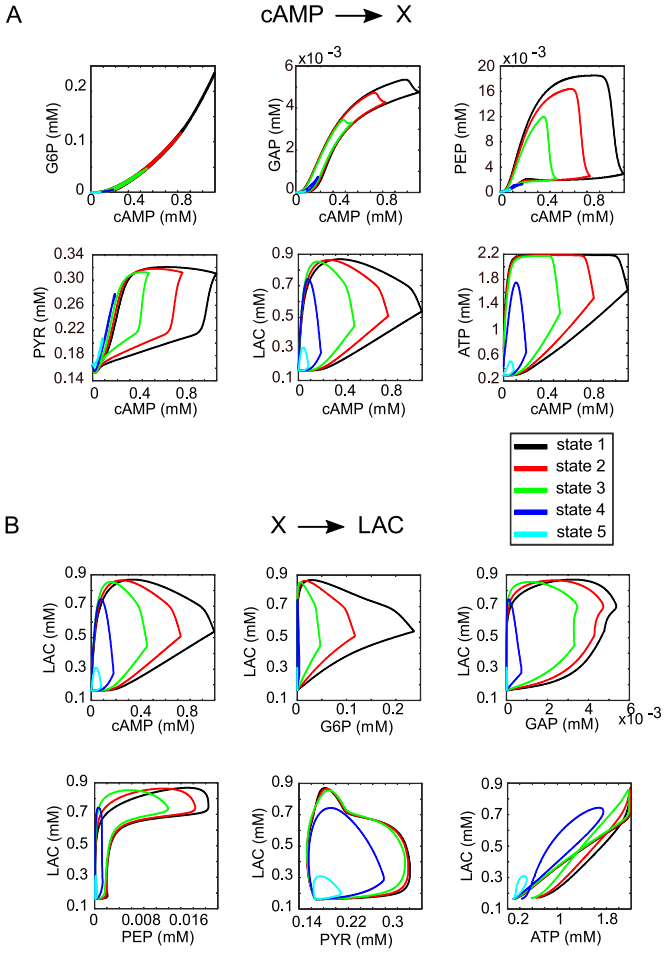

Fig. 2. Relationship between stimulus input and individual downstream cascade components (cAMP → X) and between upstream metabolites and LAC as an output example (X → LAC). A) The relationship between the cAMP stimulus and downstream metabolites may exhibit various characteristics such mirroring (as for cAMP vs. G6P), or marked hysteresis and response envelopes as for the rest. B) The relationship between various upstream cascade components and LAC as an output exhibit very different hysteresis profiles and dose-dependent phase transitions. Most of the phase transitions occur in the transition step between state 3 and 4. In the case of ATP vs. LAC, however, the normal X→ LAC hysteresis pattern is violated since LAC is not produced from ATP, but rather they are co-produced in parallel from PYR.

3 and 4 in Fig. 1. In the case of the higher dosages (green, red and black), the phase transition is manifested as responses that are growing more (but not exclusively) along the x-axis, rather than growing primarily along the y-axis in the case of the lower concentrations (cyan and blue). In the case of cAMP vs. ATP, there is also an example of a distinct ceiling to the elevation of ATP with higher doses of cAMP (near ceilings are also seen in other plots). This could have physiological implications for the cell's energy supply. As will be seen below, these state-dependent hysteresis phase plots yield rich information about the behavior of an enzymatic cascade.

Likewise, when plotting intermediate metabolites (X) vs. the downstream product of interest LAC (X→LAC), a variety of phase patterns emerge (Fig. 2B). Again, we observed that the shape of the curves qualitatively changes between the two lowest states (cyan and blue) and the higher states (green, red and black). In the case of ATP vs. LAC (last panel of Fig. 2B), the X→ LAC pattern is violated since LAC is not produced from ATP, but rather they are co-produced in parallel from PYR. In this case the phase plot takes on loops or cross-over trajectories, yet the difference in shapes, the phase transition, between the 2 lower states (cyan and blue) and the 3 higher states (green, red, black) is preserved.

3.2. State-dependent, dose-response "fingerprints"

We explored one of the implications of the 5-state hysteresis plots by selecting two independent-variable concentrations of a metabolite ("A", could be original ligand or alternative agonist) that correspond to significantly different shaped regions (indicated by the two different vertical dashed lines traversing the graphs in Fig. 3A1 and B1). We then record the corresponding output concentration of the dependent variable (metabolite "B") for each state. Points corresponding to each dashed line intersecting each hysteresis curve were plotted within corresponding color-coded bins (Fig. 3A2 and B2). We call the resulting graphs "fingerprint" plots since they provide a unique identifier of the effects of any agonist on a downstream product according to the excitation state of the given enzymatic cascade system. (We chose the relationships PEP vs. PYR and PYR vs. LAC for our samples because their hysteresis curve shapes are distinctly different and, therefore, better illustrate the usefulness of response fingerprinting). A fingerprint plot provides a way of visualizing and identifying the unique state-dependent effects of drug doses at any node (enzyme) in a metabolic network.

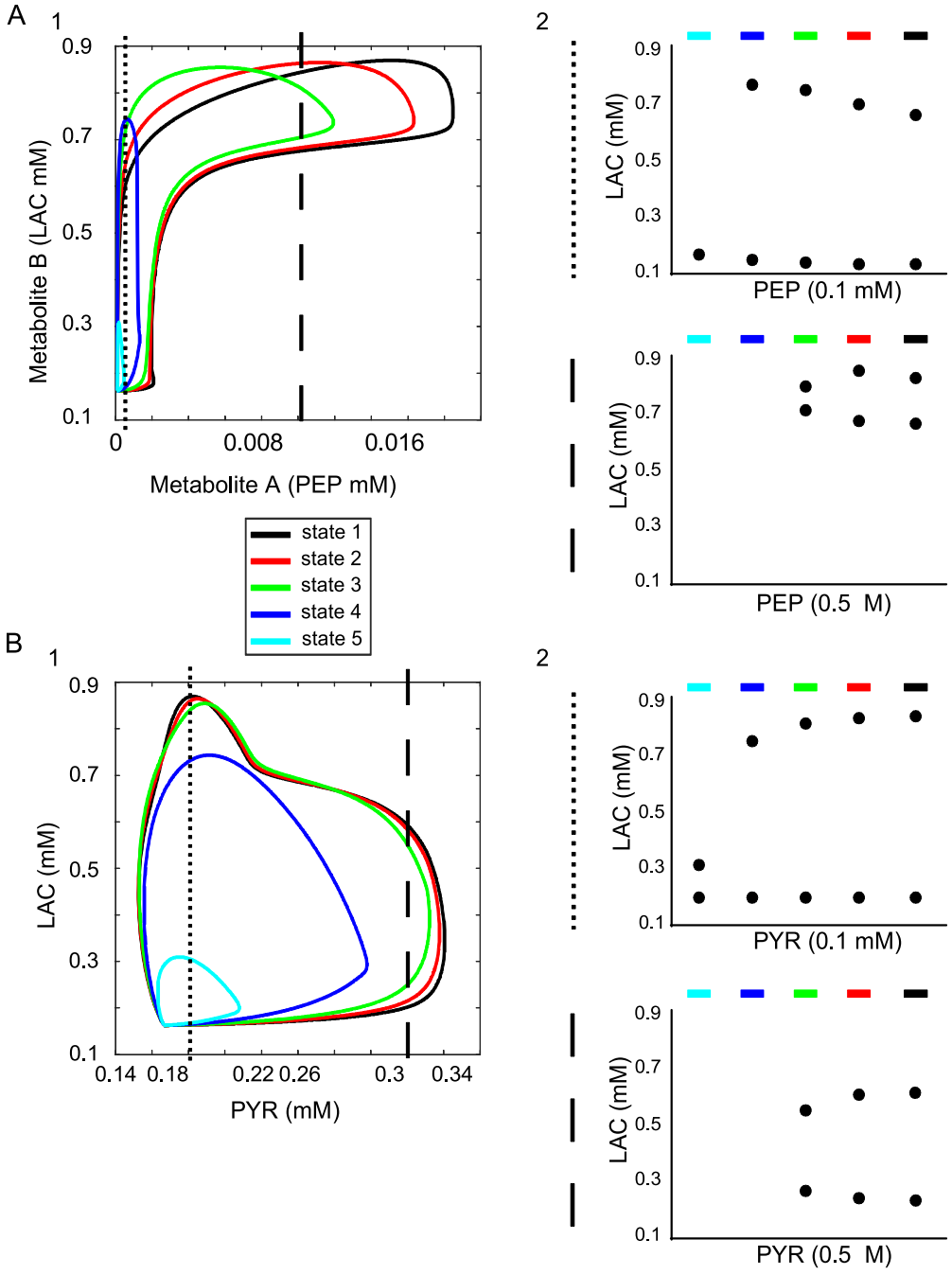

Fig. 3. State-dependent, dose-response fingerprinting. A1) With the PEP vs. LAC plot as an example, two concentrations of ligand (metabolite A) are chosen at points indicated by the two different dashed lines in order to illustrate the very different corresponding concentration responses of metabolite B, depending on the excitation state (different colors) of the system. A2) When the responses of metabolite B are plotted for each excitation state (color-coded bins) by the corresponding concentration of metabolite A, a fingerprint plot provides a way of visualizing and identifying the unique state-dependent effects of drug doses at any node (enzyme) in a metabolic network. B1 and 2) using the PYR vs. LAC relationship (as in A) to illustrate a unique fingerprint profile reflecting the very different hysteresis and phase transition for this pair of metabolites.

3.3. Production switch at bifurcation point

Both LAC and ATP can be produced at the PYR bifurcation point, with LAC being formed in the cytoplasm and ATP in the mitochondria. In our model, PYR preferentially produces ATP as seen when LAC and ATP signals are normalized by the PYR response (Fig. 4A1 and A2, respectively). Another indication of how the model equations favor the production of ATP over LAC is seen in the hysteretic trajectories of their respective phase plots. In the LAC vs. PYR plot, the phase transition between the two lower states (cyan and blue) and the three high excitation states (green, red, black) includes an inhibitory inflection, or “bite”, taken out of what would have been the trajectories of the three higher states had there been no phase transition (see solid arrow in Fig. 4A2, left panel). This inhibition of output is not seen in the corresponding excitation states for ATP vs. PYR (see dashed arrow, Fig. 4A2, right panel). There is essentially a built-in break in the production of LAC at higher concentrations of cAMP.

The PYR bifurcation point can be turned into a switch that favors the production of LAC instead of ATP. When we reduced the rate of NaK-ATPase activity by half (which reduced the need for ATP), the hysteresis curves for the higher excitation states of LAC

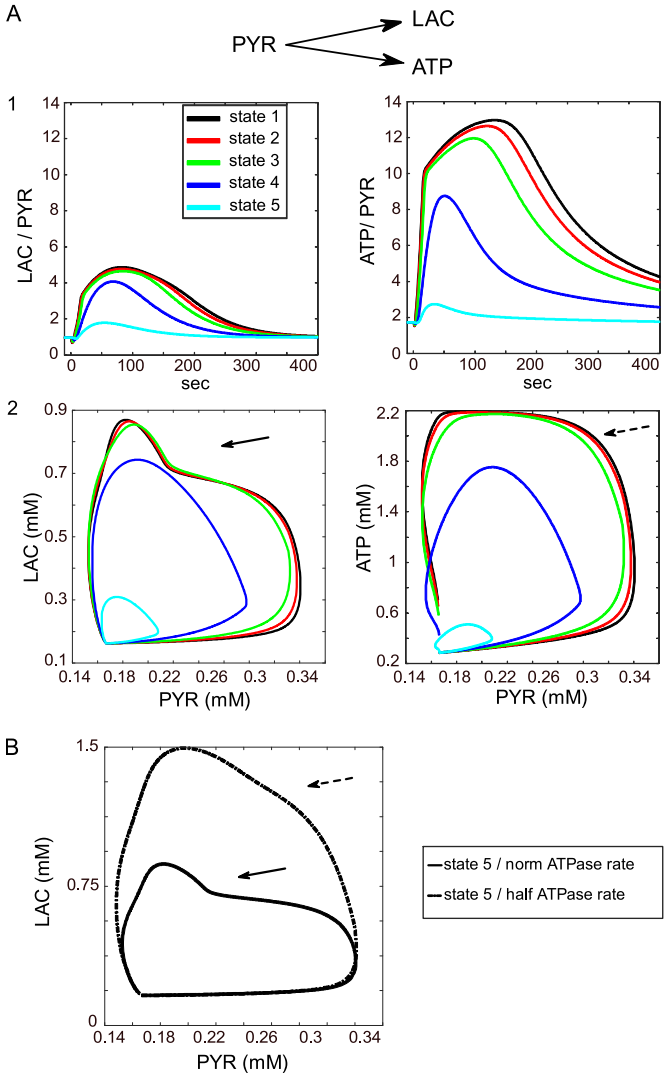

Fig. 4. Metabolic bifurcation switch: the PYR bifurcation node favors production of ATP over LAC, but can be switched to favor LAC. A1) Plots of LAC/PYR and ATP/PYR show how more ATP than LAC is produced from PYR. A2) Hysteresis plots show the difference in phase transition between states 3 and 4. The phase shift for LAC is characterized by an indentation, or bite, as indicated by the arrow. No such inhibitory inflexion is observed for the ATP phase transition. B) The profile of the phase transition for LAC can be converted to one that looks like ATP by halving the activity of the ATPase, thereby creating a bifurcation flux that favors the production of LAC over ATP.

vs. PYR no longer exhibit the inhibition "bite", but instead resemble the trajectories of the higher excitation states for ATP (compare solid and dashed arrows in Fig. 4, panels A2 and B).

3.5. 3D phase plots

We have seen how a two-dimensional plot of one metabolite vs. another in an enzymatic cascade can reveal information about the phase space of their mutual relationship, as well as the dose-dependent phase transition. We further explored the changes of shape in a three-dimensional (3D) phase space using the relationship among cAMP, PYR and LAC in one case, and cAMP, PYR and ATP in the other (metabolite selection pattern is stimulus (cAMP), bifurcation metabolite (PYR), and one or the other of the two products (ATP or LAC)). We observed a significant difference in the phase space for state 1 (Fig. 5A, z=LAC in left panel, z=ATP in right panel), where the arrows indicate the regions of greatest difference, with the inhibitory inflection, or "bite", subtracting LAC responsiveness. Much less difference between ATP and LAC were observed for state 5 (Fig. 5B), reinforcing the conclusion that at high cAMP concentrations, ATP production is favoured. The model predicts, therefore, that at ever higher metabolic stimulation, ATP production is increasingly favoured and this effect is more clearly seen in a 3D plot.

3.6. Derivative phase plots

Another way of looking at the phase transition is plotting the derivative d[L]/dt vs. the ligand, L, instead of vs. time, t (as in Fig 1F and G). These plots show the rate of change of the dependent variable concentration against the concentration itself, as well as the stable points of the system (zero intersections). Using LAC and ATP as examples, we show a clear phase transition between the lower (cyan, blue) and higher stimulated states (green, red, black) as indicated by shape change (Fig. 6A).

Visualizing the data this way gives us a more direct analogy to the dV/dt vs. V plots used to analyse AP behavior. In Fig. 6B1, an AP (upper panel) and a set of excitatory postsynaptic potentials (EPSPs) from a synapse in the Blue Brain Project's somatosensory cortex simulation are shown (Markram et al., 2015). When these time domain traces are plotted in the form dV/dt vs. V (Fig. 6B2), the resulting derivative phase plot shows the dramatic phase transition between EPSPs and the AP (as well as a subtler phase transition between the cyan/blue states and the green/red states, suggesting two phase transitions for these APs).

3.7. Molecular phase signalling hypothesis

The main point here, however, is not the total number of phases in the EPSP to AP transition vs. the low-state to high-state ligand-pulse (LP) transition, but that the LPs are similar in concept with the AP, which is essentially a voltage pulse. Different "doses" of voltage govern whether the response is a subthreshold EPSP or a suprathreshold AP, whereas different doses of a ligand concentration determine whether a subthreshold concentration trajectory or a suprathreshold ligand pulse is generated. In both cases, a set of enzymes forms a system that is involved in a cooperative phenomenon we call "molecular phase signalling" (MPS). A summary of our molecular phase signalling hypothesis is provided in Fig. 7.

4. Discussion

With a computational model of energy metabolism, we demonstrate how an enzymatic cascade may operate as a functional unit of interdependent reactions rather than just a series of independent reaction steps. Stimulation of these systems can produce emergent effects such as state or phase transitions that could act as signalling mechanisms, thus expanding the overall information processing possibilities for biochemical reaction networks. We applied this novel analysis of stimulated second-messenger enzyme cascades to energy metabolism in glia. Astrocytes can be stimulated by the neuromodulator NE to induce glycogenolysis via a cAMP-dependent, second-messenger transduction mechanism (Coggan et al., 2018; Subbarao and Hertz, 1990), with higher levels of NE stimulation resulting in corresponding increases in intracellular concentrations of cAMP (Fig. 1B). When we look at downstream metabolite levels or their rate of formation, however, we see a change in the response trajectory, or phase transition, between the lower two concentrations of cAMP and the higher three (e.g., for LAC and ATP, Figs. 1 D, E for concentrations and 1 F, G, for rates of formation, respectively).

Hysteretic trajectories are observed when plotting cAMP vs. downstream metabolites or between upstream metabolites and

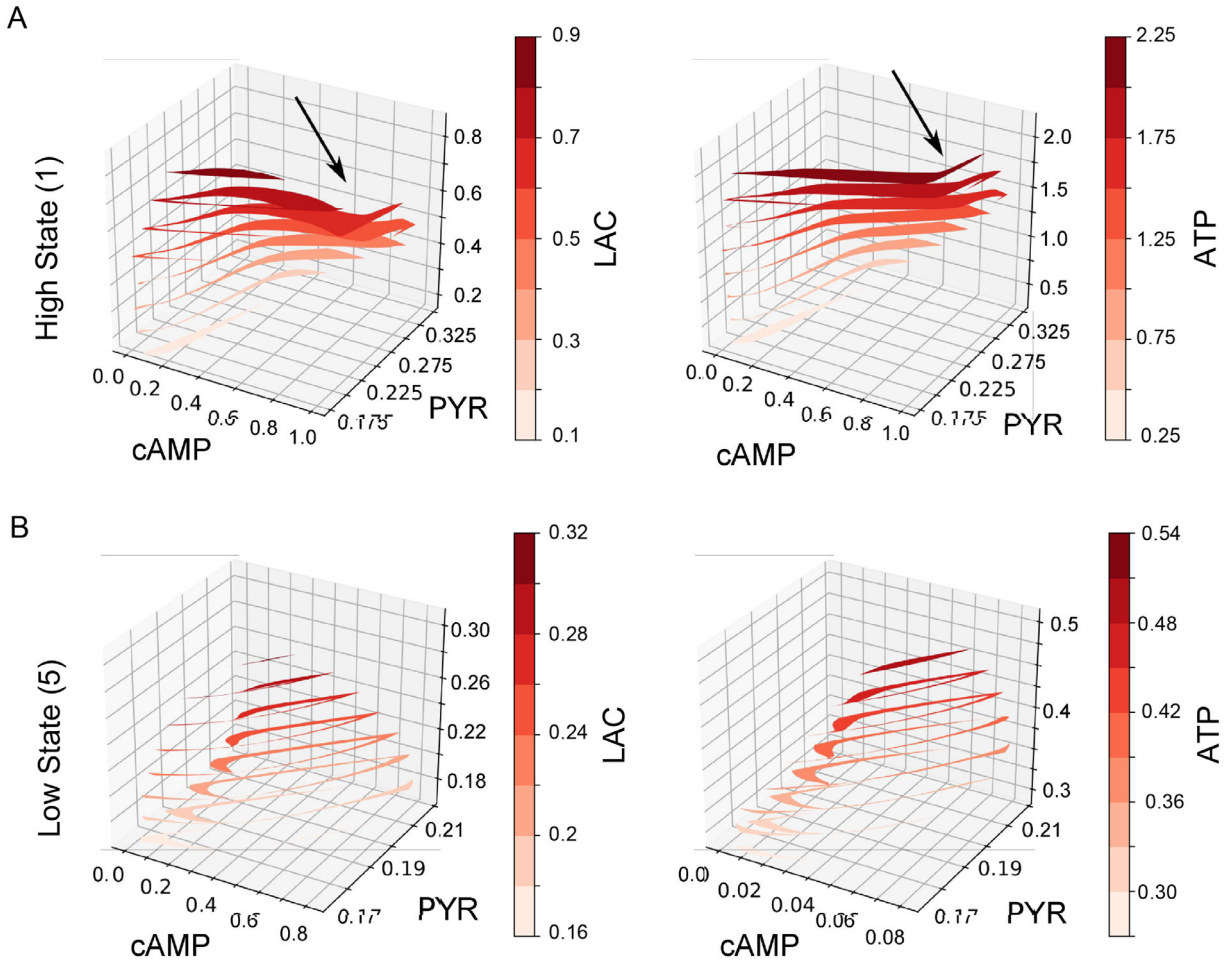

Fig. 5. 3D analysis shows the favored production of ATP is prominent at high metabolic network states. A) at high metabolic excitation state 1, there is a pronounced difference between ATP and LAC production when plotted in the same 3D parameter space as cAMP and PYR. Arrow points to empty region ("bite") signifying inhibition in the production of LAC. B) At lowest metabolic excitation state 5, while there is still more ATP produced, the effect is considerably smaller. The model predicts, therefore, that at ever higher metabolic stimulation, ATP production is increasingly favoured and this effect is more clearly seen in a 3D plot.

LAC, our metabolite of interest (Fig. 2). Data viewed in this way confirms the phase transitions at higher doses of cAMP and offers a new way of understanding the complex relationships between any two metabolites involved in a cascade system. For our model, the implication is that higher energy mobilization regimes are entered at the highest stimulation levels. In addition, the striking similarity to the phase transition between EPSPs and APs suggests additional information carrying capabilities of metabolic systems (Fig. 6) that further experiments will continue to explore.

Altogether, given the ubiquitous presence and multipurpose roles of second-messenger transduction systems, our analysis outlines a novel approach that should provide a better theoretical foundation for understanding signalling cascades. This gained competence has implications for understanding the breadth and efficiency of biological computations and illuminates a pathway towards more efficient synthetic biology practices.

4.1. Implications of phase or state transitions in hysteresis plots

Hysteresis in the relationship between ligands in a cascade can be viewed as a form of system memory containing information about recent stimulation states. Glycolytic hysteresis has been proposed as a mechanism that compounds age-related neurodegeneration by synergetic mechanisms, since glycolytic gene upregulation in response to glucose drains cellular redox capacity (Mobbs et al., 2007). Our results suggest that hysteresis memory can be more complicated than previously considered, involving any number of inter-dependent steps, and requiring computational analysis to sort out. Hysteresis patterns in our model undergo dose-dependent phase transitions that report information about neuromodulatory stimulation levels.

The meaning of phase transition varies by context, but the common idea here is a threshold separating distinct behaviors of a system. The properties of non-equilibrium steady-state phase transitions (NESS) are the same as for those equilibrated (Ge and Qian, 2011, Yang and Lee, 1952), which is fortunate since biological reaction systems are usually not in equilibrium. In biology, there are numerous examples such as the phase transitions that lead to intracellular molecular condensations (Holehouse and Pappu, 2018). Here we explored a way of analysing a relatively large set of chain-linked, stimulation level-driven, equations describing a molecular cascade and showed a type of dose-dependent phase transition akin to that exhibited by the transition from EPSPs to APs – a phase transition encoded in the Hodgkin-Huxley derived relationships for specific ion channels that form a cooperative system for producing an AP.

An ion channel can be thought of as a voltage-dependent enzyme trapped in a lipid-bilayer membrane. The excitability state of neurons in an engram, determined by ion channel states, may alter the retrieval strength of a memory or a behavioural outcome (Pignatelli et al., 2019, Aizenman and Linden, 2000). We propose

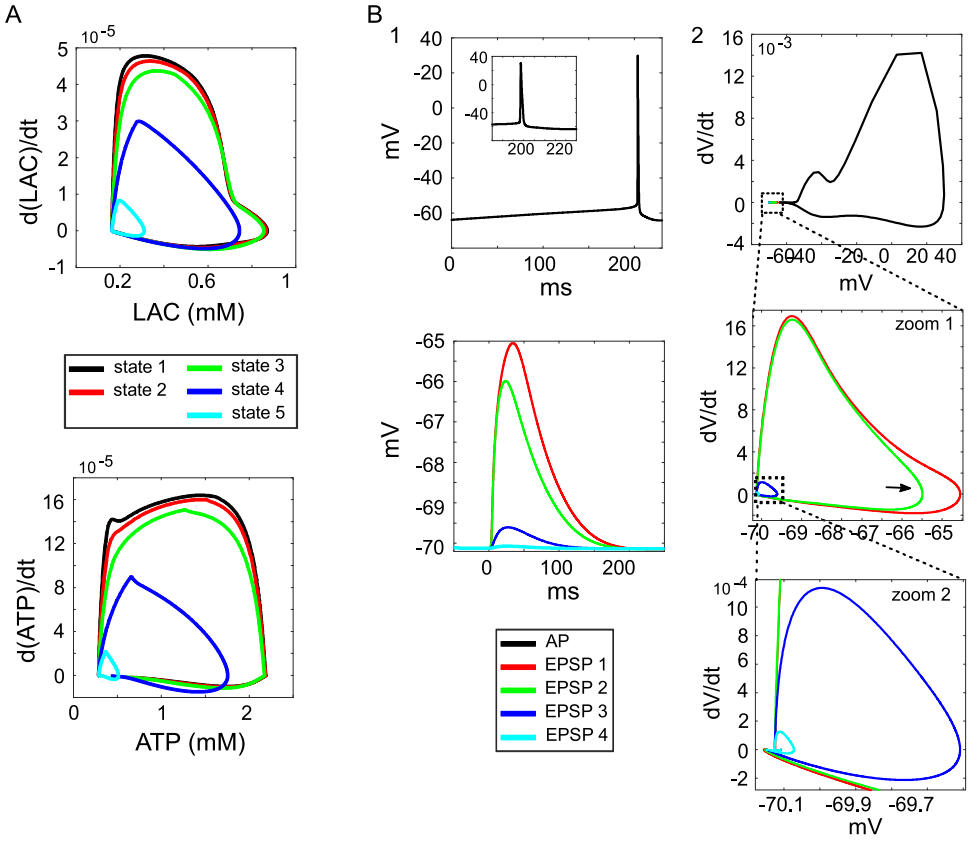

Fig. 6. Ligand-pulse phase signalling: the behaviour of metabolic cascades at multiple levels of excitation resembles that of the transition between EPSPs and APs. A) with d[L]/dt vs. L phase plots (where L = ligand) for LAC, top, and ATP, bottom. B1) Action potential (AP), with zoom inset, taken from simulation of neuron from the Blue Brain Project's somatosensory cortex (upper plot) and a set of EPSPs generated from increasing levels of synaptic strength in the same neuron prior to spiking. B2) dV/dt vs. V plots for the EPSPS and AP in A with successive zooms to show shapes of EPSP phase plots. Arrow points to lag in filling in one of the lobes of the hysteresis shape. Note shapes of weakest EPSP plots (cyan and blue) are a different shape than two mid-size (green and red) and radically different from the shape of the AP trajectory (black). An AP can be thought of as a "voltage -pulse" phase signal just as a suprathreshold concentration of ligand produces a "ligand pulse".

that the excitability state of a metabolic cascade might similarly retain information.

4.2. State-dependent, dose-response "fingerprints"

Standard practice for most pharmaceutical drug discovery is to focus on the effects of a therapeutic molecule candidate in a single enzyme assay, looking for a change in a particular downstream effect to determine a mechanism of action (MOA) (Hughes et al., 2011). This approach has proven largely ineffective when applied to the development of pharmacotherapies for many diseases underlaid by complex biochemistry such as cancer and most brain disorders. While multiple drug targets might prove more effective, there has been relatively scant attention paid to this approach (Thai et al., 2017), likely for the lack of employment of computational methods.

Incorporating an understanding of non-linear properties of metabolic systems would benefit the drug discovery processes since many disease states are related to dynamical dysfunctions that might require multiple therapeutic targets (Aradi and Erdi, 2006, Belair et al., 1995, Coggan et al., 2015, van der Greef and McBurney, 2005). For example, the behavior of biochemical cascades in single cells is likely to influence synapses and neural networks (Destexhe and Marder, 2004). Synthetic biology research and applications also increasingly require computational models to efficiently design or optimize production (Teusink and Smid, 2006) and are in sore need of tools to predict outcomes of manipulations (Costello and Martin, 2018).

Our model shows that the behaviour of any given enzyme in a cascade, or metabolite concentration, will depend on the level to which the entire system is stimulated. By designing assays for response fingerprinting, a drug's efficacy and specificity might be better pinpointed. In addition, a clear path to a drug cocktail approach might be indicated by better understanding how the system responds to perturbations, as has been suggested in a computational model of multiple sclerosis (Coggan et al., 2010).

4.3. Synthetic biology

Simulation science could complement the efforts already well-underway for optimising the output of useful compounds using microorganisms by saving time and indentifying solutions (Martin et al., 2009). In the case of *S. cerevisiae*, for example, NADPH synthetic pathways have been tweaked to increase production goals for pharmaceutical agents (Kim et al., 2018). The molecular switch we demonstrate in Fig. 4, for example, demonstrates the effectiveness of computational models for predicting yields and optimal intervention sites in metabolic pathways. While bistability in general, and in the glycolytic pathway in particular, has been observed and proposed as metabolic switch (Mulukutla et al., 2014, Ferrell and Xiong, 2001), we propose that the excitation state of any given system of enzymes, of arbitrary size, will affect the existence or loci of bistability sites and that computational models can reveal or predict these points.

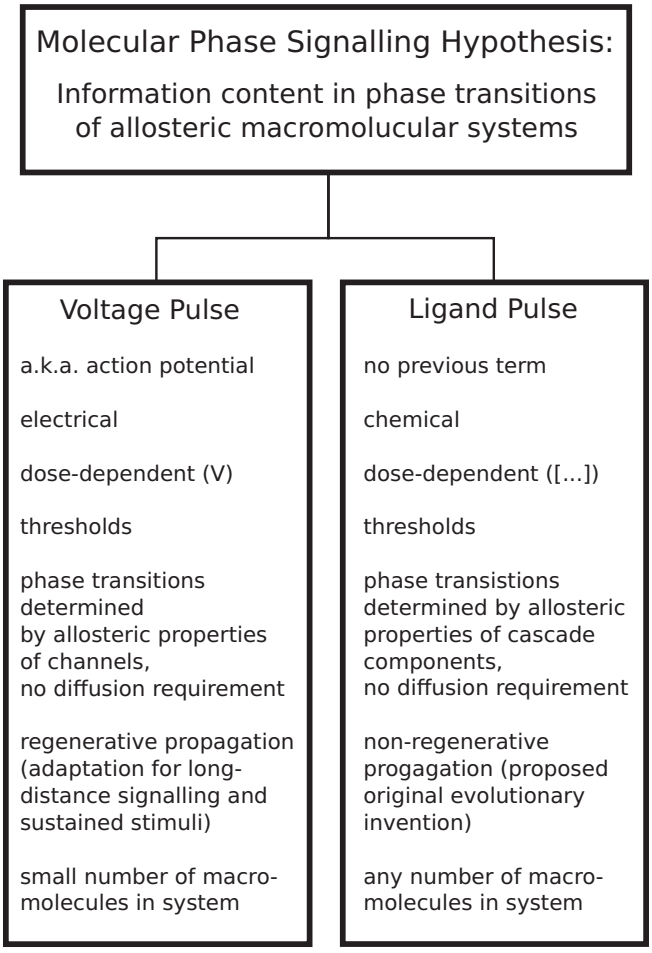

Fig. 7. Summary of Molecular Phase Signalling hypothesis. In this theory, a dose-sensitive phase transition in the hysteretic response trajectory provides information about the state of the system of enzymes, whether a small set that responds to a voltage dose, or a larger set in a metabolic cascade where nodes respond to ligand doses. In the case of metabolite concentrations, the ligand pulse conveys the information. In the case of electric potentials, a voltage pulse (a.k.a., action potential) carries the information. This theory could imply an evolutionary link between APs and LPs based on the behaviors of sets of allosteric macromolecules that constitute a system.

4.4. Molecular phase signalling and "ligand pulses"

The metabolite production of a simulated enzymatic cascade is encoded in the set of differential equations and exhibit emergent, dose-dependent phase transitions. The idea that the phase transition contains information in the form of a pulse of ligand (the LP) reminded us of the voltage pulses also known as APs. The AP has ancient evolutionary roots in both bikonta and unikonta (Brunet and Arendt, 2016), the predecessors of plants, fungi and animals, and various other eukaryotes, any may have roots down to the last eukaryotic common ancestor (LECA) or even before. More recently in evolution, this voltage cycling mechanism may have been repurposed for rapid or long distance signalling in modern nervous systems (Pineda and Ribera, 2007).

The authors propose that LPs could represent an evolutionarily conserved, pre-LECA, molecular phase signalling mechanism (see Fig. 7), from which APs were adapted for voltage regulation, contraction or communication between electrically excitable cells. It has been thought at least since the 1940s that all multicellular system functions have their roots in single celled ancestors (cf. works of GG Simpson, e.g. (Simpson, 1945)). Phase analysis of intracellular signal transduction could be a very useful partner to experimentalists trying to precisely measure and understand the significance of fluctuations of metabolites in single cells, not only neurons, but even bacteria and other cells (Potvin-Trottier et al., 2018). Evidence for the involvement of glia in behaviour begs the question of the nature of information processing in non-spiking cells and their coupling mechanisms to neurons in heterocelluar communication (Mu et al., 2019, Lalo et al., 2011).

AP- or LP-type phenomena in single-celled organisms also support our hypothesis. For example, bacterial biofilms can produce potassium-based depolarization waves for communication within their community system (Prindle et al., 2015) - the possible unifying principle being that a group of enzymes, including ion channels, can cooperate to achieve an information processing unit in a state-dependent manner (Ågren et al., 2019).

We offer several conclusions or predictions from our metabolic cascade model analysis, including: 1) A cascade chain of enzymes may be considered a system that can exist in multiple simulated states, and these states inform their functional properties; 2) Cascade states can result in dose-response "fingerprinting"; 3) Dose-dependent phase transitions in a cascade can carry information analogous to EPSPs (if subthreshold) or APs (if suprathreshold), resulting in a theory of "ligand-pulse" (LP) molecular phase signalling.

We further speculate that enzyme cascades might contribute to energy efficient computing in the brain by bestowing on single cells a new dimension of information processing capability. This idea, in turn, challenges preconceptions about what and where a brain is computing.

Funding

Funding: King Abdullah University of Science and Technology (grant number 2313) Swiss Federal Institutes of Technology Board (ETH Board) École polytechnique fédérale de Lausanne (EPFL); This study was supported by funding to the Blue Brain Project, a research center of the École polytechnique fédérale de Lausanne, from the Swiss government's ETH Board of the Swiss Federal Institutes of Technology (HM); NCCR Synapsy (PJM); and the Prefargier Foundation (PJM). The funders had no involvement in the study design, in the collection, analysis and interpretation of data, in the writing of the report, nor in the decision to submit the article for publication.

Declaration of Competing Interest

None.

CRediT authorship contribution statement

Jay S Coggan: Conceptualization, Writing - original draft. **Daniel Keller:** Conceptualization, Writing - original draft. **Henry Markram:** Supervision, Funding acquisition. **Felix Schürmann:** Supervision, Funding acquisition. **Pierre J Magistretti:** Supervision, Funding acquisition.

Acknowledgements

We thank Werner Van Geit for the AP and EPSP data from the Blue Brain Project's cortical column microcircuit simulation and Lida Kanari for Python scripts used in the 3D data plots.

References

Ågren, R., Nilsson, J., Århem, P., 2019. Closed and open state dependent block of potassium channels cause opposing effects on excitability – a computational approach. Sci. Rep. 9. doi:10.1038/s41598-019-44564-x.

Aizenman, C.D., Linden, D.J., 2000. Rapid, synaptically driven increases in the intrinsic excitability of cerebellar deep nuclear neurons. Nat. Neurosci. 3, 109–111. doi:10.1038/72049.

Aradi, I., Erdi, P., 2006. Computational neuropharmacology: dynamical approaches in drug discovery. Trends Pharmacol. Sci. 27, 240–243. doi:10.1016/j.tips.2006.03.004.

Belair, J., Glass, L., An Der Heiden, U., Milton, J., 1995. Dynamical disease: Identification, temporal aspects and treatment strategies of human illness. Chaos 5, 1–7. doi:10.1063/1.166069.

Boyer, M., Wisniewski-Dyé, F., 2009. Cell–cell signalling in bacteria: not simply a matter of quorum: Cell–cell signalling in bacteria. FEMS Microbiol. Ecol. 70, 1–19. doi:10.1111/j.1574-6941.2009.00745.x.

Brunet, T., Arendt, D., 2016. From damage response to action potentials: early evolution of neural and contractile modules in stem eukaryotes. Philos. Trans. R. Soc. B Biol. Sci. 371, 20150043. doi:10.1098/rstb.2015.0043.

Coggan, J.S., Bittner, S., Stiefel, K.M., Meuth, S.G., Prescott, S.A., 2015. Physiological dynamics in demyelinating diseases: unraveling complex relationships through computer modeling. Int. J. Mol. Sci. 16, 21215–21236. doi:10.3390/ijms160921215.

Coggan, J.S., Keller, D., Calì, C., Lehväslaiho, H., Markram, H., Schürmann, F., et al., 2018. Norepinephrine stimulates glycogenolysis in astrocytes to fuel neurons with lactate. PLoS Comput. Biol. 14, e1006392. doi:10.1371/journal.pcbi.1006392.

Coggan, J.S., Prescott, S.A., Bartol, T.M., Sejnowski, T.J., 2010. Imbalance of ionic conductances contributes to diverse symptoms of demyelination. Proc. Natl. Acad. Sci. USA 107, 20602–20609. doi:10.1073/pnas.1013798107.

Costello, Z., Martin, H.G., 2018. A machine learning approach to predict metabolic pathway dynamics from time-series multiomics data. NPJ Syst. Biol. Appl. 4. doi:10.1038/s41540-018-0054-3.

DeBerardinis, RJ, Thompson, CB, 2012. Cellular metabolism and disease: what do metabolic outliers teach us? Cell 148, 1132–1144. doi:10.1016/j.cell.2012.02.032.

Destexhe, A, Marder, E., 2004. Plasticity in single neuron and circuit computations. Nature 431, 789–795. doi:10.1038/nature03011.

Erb, TJ, Jones, PR, Bar-Even, A, 2017. Synthetic metabolism: metabolic engineering meets enzyme design. Curr Opin Chem Biol 37, 56–62. doi:10.1016/j.cbpa.2016.12.023.

Ferrell, J.E., Xiong, W., 2001. Bistability in cell signaling: How to make continuous processes discontinuous, and reversible processes irreversible. Chaos 11, 227–236. doi:10.1063/1.1349894.

Ge, H., Qian, H., 2011. Non-equilibrium phase transition in mesoscopic biochemical systems: from stochastic to nonlinear dynamics and beyond. J. R. Soc. Interface 8, 107–116. doi:10.1098/rsif.2010.0202.

Holehouse, AS, Pappu, RV., 2018. Functional implications of intracellular phase transitions. Biochemistry 57, 2415–2423. doi:10.1021/acs.biochem.7b01136.

Hughes, J., Rees, S., Kalindjian, S., Philpott, K., 2011. Principles of early drug discovery: Principles of early drug discovery. Br. J. Pharmacol. 162, 1239–1249. doi:10.1111/j.1476-5381.2010.01127.x.

Jolivet, R., Coggan, J.S., Allaman, I., Magistretti, P.J., 2015. Multi-timescale modeling of activity-dependent metabolic coupling in the neuron-glia-vasculature ensemble. PLoS Comput. Biol. 11, e1004036. doi:10.1371/journal.pcbi.1004036.

Kim, J.-E., Jang, I.-S., Sung, B.H., Kim, S.C., Lee, J.Y., 2018. Rerouting of NADPH synthetic pathways for increased protopanaxadiol production in Saccharomyces cerevisiae. Sci. Rep. 8, 15820. doi:10.1038/s41598-018-34210-3.

Kirkwood, T.B.L., 2011. Systems biology of ageing and longevity. Philos. Trans. R. Soc. Lond. B Biol. Sci. 366, 64–70. doi:10.1098/rstb.2010.0275.

Kowald, A., Kirkwood, T.B., 1996. A network theory of ageing: the interactions of defective mitochondria, aberrant proteins, free radicals and scavengers in the ageing process. Mutat. Res. 316, 209–236.

Kriete, A., Lechner, M., Clearfield, D., Bohmann, D., 2011. Computational systems biology of aging. Wiley Interdiscip. Rev. Syst. Biol. Med. 3, 414–428. doi:10.1002/wsbm.126.

Lalo, U., Pankratov, Y., Parpura, V., Verkhratsky, A., 2011. Ionotropic receptors in neuronal-astroglial signalling: what is the role of “excitable” molecules in non-excitable cells. Biochim. Biophys. Acta 1813, 992–1002.

Markram, H, Muller, E, Ramaswamy, S, Reimann, MW, Abdellah, M, Sanchez, CA, et al., 2015. Reconstruction and simulation of neocortical microcircuitry. Cell 163, 456–492. doi:10.1016/j.cell.2015.09.029.

Martin, C.H., Nielsen, D.R., Solomon, K.V., Prather, K.L.J., 2009. Synthetic metabolism: engineering biology at the protein and pathway scales. Chem. Biol. 16, 277–286. doi:10.1016/j.chembiol.2009.01.010.

Mc Auley, M.T., Guimera, A.M., Hodgson, D., Mcdonald, N., Mooney, K.M., Morgan, A.E., et al., 2017. Modelling the molecular mechanisms of aging. Biosci. Rep. 37. doi:10.1042/BSR20160177, BSR20160177.

Mobbs, C.V., Mastaitis, J.W., Zhang, M., Isoda, F., Cheng, H., Yen, K., 2007. Secrets of the lac operon. Glucose hysteresis as a mechanism in dietary restriction, aging and disease. Interdiscip. Top. Gerontol. 35, 39–68. doi:10.1159/000096555.

Mu, Y, Bennett, DV, Rubinov, M, Narayan, S, Yang, C-T, Tanimoto, M, et al., 2019. Glia accumulate evidence that actions are futile and suppress unsuccessful behavior. Cell doi:10.1016/j.cell.2019.05.050.

Mulukutla, BC, Yongky, A, Daoutidis, P, Hu, W-S, 2014. Bistability in glycolysis pathway as a physiological switch in energy metabolism. In: Dzeja, P (Ed.). In: PLoS One, 9, p. e98756. doi:10.1371/journal.pone.0098756.

Mulukutla, BC, Yongky, A, Grimm, S, Daoutidis, P, Hu, W-S, 2015. Multiplicity of Steady states in glycolysis and shift of metabolic state in cultured mammalian cells. In: Coles, JA (Ed.). PLoS One, 10 editor doi:10.1371/journal.pone.0121561.

Mulukutla, B.C., Yongky, A., Le, T., Mashek, D.G., Hu, W.-S., 2016. Regulation of glucose metabolism – a perspective from cell bioprocessing. Trends Biotechnol. 34, 638–651. doi:10.1016/j.tibtech.2016.04.012.

Nedelsky, N.B., Taylor, J.P., 2019. Bridging biophysics and neurology: aberrant phase transitions in neurodegenerative disease. Nat. Rev. Neurol. doi:10.1038/s41582-019-0157-5.

Pignatelli, M, Ryan, TJ, Roy, DS, Lovett, C, Smith, LM, Muralidhar, S, et al., 2019. Engram cell excitability state determines the efficacy of memory retrieval. Neuron 101, 274–284. doi:10.1016/j.neuron.2018.11.029, e5.

Pineda, RH, Ribera, AB., 2007. Evolution of the action potential. In: Evolution of Nervous Systems. Elsevier, pp. 211–238. doi:10.1016/B0-12-370878-8/00119-1.

Potvin-Trottier, L., Luro, S., Paulsson, J., 2018. Microfluidics and single-cell microscopy to study stochastic processes in bacteria. Curr. Opin. Microbiol. 43, 186–192. doi:10.1016/j.mib.2017.12.004.

Prindle, A, Liu, J, Asally, M, Ly, S, Garcia-Ojalvo, J, Süel, GM, 2015. Ion channels enable electrical communication in bacterial communities. Nature 527, 59–63. doi:10.1038/nature15709.

Schoeberl, B., Eichler-Jonsson, C., Gilles, E.D., Müller, G., 2002. Computational modeling of the dynamics of the MAP kinase cascade activated by surface and internalized EGF receptors. Nat. Biotechnol. 20, 370–375. doi:10.1038/nbt0402-370.

Simpson, G.G., 1945. Tempo and mode in evolution. Trans. N. Y. Acad. Sci. 8, 45–60.

Subbarao, K.V., Hertz, L., 1990. Effect of adrenergic agonists on glycogenolysis in primary cultures of astrocytes. Brain Res 536, 220–226. doi:10.1016/0006-8993(90)90028-a.

Teusink, B., Smid, E.J., 2006. Modelling strategies for the industrial exploitation of lactic acid bacteria. Nat. Rev. Microbiol. 4, 46–56. doi:10.1038/nrmicro1319.

Thai, N.Q., Nguyen, H.L., Linh, H.Q., Li, M.S., 2017. Protocol for fast screening of multi-target drug candidates: application to Alzheimer's disease. J. Mol. Graph. Model. 77, 121–129. doi:10.1016/j.jmgm.2017.08.002.

Tsuruyama, T., 2014. A Model of Cell Biological Signaling Predicts a Phase Transition of Signaling and Provides Mathematical Formulae. In: Xu, Y (Ed.). PLoS One, 9 editor doi:10.1371/journal.pone.0102911.

van der Greef, J., McBurney, R.N., 2005. Innovation: rescuing drug discovery: in vivo systems pathology and systems pharmacology. Nat. Rev. Drug Discov. 4, 961–967. doi:10.1038/nrd1904.

Yang, C.N., Lee, T.D., 1952. Statistical theory of equations of state and phase transitions. I. Theory of condensation. Phys. Rev. 87, 404–409. doi:10.1103/PhysRev.87.404.